THE JOURNAL OF PHYSICAL CHEMISTRY A

 VOLUME 107, NUMBER 13, APRIL 3, 2003

ARTICLES

The Internal Energy of Neutral Ethylene Glycol Molecules Created in the Laser Vaporization of Aerosol Particles

Ephraim Woods III,† Roger E. Miller,* and Tomas Baer*

Department of Chemistry,University of North Carolina, Chapel Hill, North Carolina 27599-3290

Received: August 7, 2002; In Final Form: January 13, 2003

Although laser vaporization of aerosol particles plays an important role in aerosol mass spectrometry, relatively little is known about disposal of excess energy in the degrees of freedom of the gas-phase species. A two-laser scheme, in which an infrared laser vaporizes aerosol particles prior to ionization of the vapor plume by a vacuum-ultraviolet laser, permits the determination of the internal energy of the neutral molecules created in laser vaporization. In this work, the fragmentation patterns of vacuum UV (VUV) photoionization mass spectra of ethylene glycol, in conjunction with photoelectron-photoion coincidence (PEPICO) measurements, determines the internal energy of gas-phase molecules created in the CO_2 laser vaporization of neat ethylene glycol particles and ethanol particles mixed with trace ethylene glycol. The internal energy ranges from 1300 to 10250 cm^{-1} for CO_2 laser powers between 25 and 112 mJ/pulse. For neat ethylene glycol, the rate with which the internal and kinetic energy grows with laser power increases sharply above 65 mJ/pulse, consistent with a change in vaporization mechanism from thermal to explosive. Monitoring the total ion signal as a function of the delay between the CO_2 and VUV lasers provides an estimate of the relative kinetic energy of the vaporized molecules. At high laser fluences, the estimated translational energy is greater than the corresponding internal energy, indicative of vibrational cooling in the vapor plume. Ethanol particles containing 1.0% ethylene glycol produce similar results, with the transition in heating rate occurring at a lower temperature. The simplicity of the fragmentation pattern in these spectra and the broad range of temperatures that can be measured in this fashion make ethylene glycol an excellent "chemical thermometer" for reactions initiated by the laser heating of aerosol particles.

Introduction

Several implementations of aerosol mass spectrometry rely on the laser ablation of aerosols to generate gas-phase species suitable for mass analysis. Despite the importance of the ablation process in the performance of these spectrometers, the mechanisms for laser ablation of aerosols have only recently been investigated. Both imaging experiments[1−3] and molecular dynamics simulations[4,5] show a transition between a thermal, layer-by-layer evaporation at low laser fluences to a more explosive evaporation involving the mass removal of material from the particle at high laser fluences. A similar transition from thermal to explosive vaporization has been implicated in a depth-profiling study of coated aerosol particles.[6]

Comparatively little is known about the partitioning of the excess energy in the gas-phase molecules. In particular, there have been no studies that describe the internal energy of the gas-phase molecules created in aerosol particle ablation. Nevertheless, the internal energy is an important parameter in

* Corresponding authors. Fax: (919)962-2388. E-mail: baer@unc.edu; remiller@unc.edu.

† Current address: Department of Chemistry, Colgate University, 13 Oak Drive, Hamilton, NY 13346.

10.1021/jp0218387 CCC: $25.00
Published on Web 03/06/2003

analytical aerosol mass spectrometry because it controls both fragmentation in mass spectra and contributes to ion−molecule reactions, known as "matrix effects". Furthermore, a new technique that probes the initial stages of combustion in explosive aerosol particles also uses single particle mass spectrometry.[7] In this technique, an infrared laser initiates chemical reactions in the particle as it evaporates, and the temperature reached by the superheated particle controls the pathways and rates of the reactions. An independent measure of the internal temperature would provide important information for these studies. For example, it would provide a means to distinguish energy imparted by the laser and the energy released by the exothermic reaction.

Although no experimental studies have been reported regarding the internal energy of laser-vaporized aerosol particles, a few studies have measured the internal energy of molecules ejected by ablation from a macroscopic matrix. Mowry and Johnston measured the vacuum UV (VUV) photoionization mass spectrum of primary and secondary alkylamines following matrix-assisted laser desorption (MALD).[8] They used the extent of fragmentation in the spectra as a measure of the average internal energy, and found between 0.6 and 0.9 eV (440−520 K) for desorption laser irradiances near threshold. They also observed that high internal energies were correlated with high translational energies. Zhang et al.[9] probed neutral benzimidazole ejected from a water/glycerol matrix by a CO_2 laser using resonant two-photon ionization (R2PI). They found significant cooling of the vibrational modes (43 K), indicative of the formation of a free jet expansion at the desorbing surface. In this case, the internally cold molecules were translationally hot, whereas the internally excited molecules were translationally cold. In a similar study, Elokhin et al.[10] used R2PI to observe vibrational cooling in aniline molecules ejected from a cryogenic matrix by CO_2 laser ablation. The internal temperature of the aniline molecules was estimated to be 170 K, slightly colder than the temperature of the matrix. Finally, Cousins et al.[11] observed translationally hot, but internally unexcited NO molecules from the 193-nm laser ablation of multilayer, cryogenic NO films.

In this work, we measure the internal energy imparted to ethylene glycol molecules in the CO_2 laser vaporization of neat ethylene glycol aerosol particles in a vacuum. We use the fragmentation pattern from VUV photoionization mass spectra of the ethylene glycol vapor plume to measure the internal energy, similar to the approach of Mowry and Johnston[8] in their matrix-assisted laser desorption-photoionization (MALD-PI) study. However, we integrate data from photoelectron-photoion-coincidence (PEPICO) measurements and the room-temperature photoelectron spectrum into our analysis, making the internal energy determination more accurate.

The goal of this work is an improved understanding of the energy partitioning among internal and translational degrees of freedom in the vaporization dynamics. Additionally, characterizing the relationship between the photoionization mass spectrum and the internal energy distribution of the neutral precursors provides a "chemical thermometer" for use in other systems. Ethylene glycol, or another molecule whose fragmentation patterns are well-characterized, may be added in small concentrations to reactive systems such as our recently investigated combustion of nitromethane aerosol,[7] and used to evaluate the reaction's "temperature". In addition, the mass spectral fragmentation patterns obtained by the addition of trace amounts of ethylene glycol in other ionization processes such as laser ablation or MALDI (mass-analyzed laser desorption ionization) can be used to determine the internal energy distribution of the resulting ions.

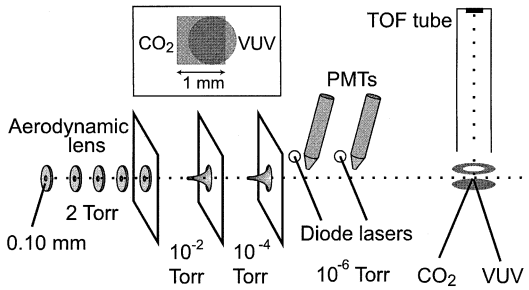

Figure 1. The experimental arrangement of the aerosol mass spectrometer. The diode laser light scattering signals measure the particle velocity. The CO_2 laser vaporizes the particle, and the vacuum UV (VUV) laser ionizes the gas-phase species, whose time-of-flight is measured. The insert shows the overlap of the CO_2 and VUV laser beams.

Experiment

The arrangement of the present experiment, shown schematically in Figure 1, is similar to that described in previous papers from this laboratory.[6,7,12] It differs from other laser aerosol time-of-flight mass spectrometers[13−15] used for on-line analysis of atmospheric aerosol particles in that separate vaporization and ionization lasers are used to create the ions for mass analysis. The system comprises an aerodynamic lens inlet, two stages of differential pumping, a light scattering station, and a laser-based time-of-flight mass spectrometer. Aerosol particles (2 μm in diameter) from an external gas stream enter the aerodynamic lens through a 100 μm, flow-limiting orifice. The aerodynamic lens consists of a series of orifices of successively decreasing diameter, a design based on the work of McMurry and co-workers.[16,17] The lens focuses aerosol particles onto a well-defined axis, greatly increasing the efficiency with which we detect them. The focused particles accelerate through two stages of differential pumping to speeds of approximately 100 m/s before entering the chamber containing the time-of-flight mass spectrometer. The particles then pass through two 532 nm diode laser beams placed 10 cm apart. Separate photomultiplier tubes detect the scattered light from the diode lasers, and a digital timing circuit calculates the velocity of the particle on the basis of the time delay between the two scattered light signals. The circuit then triggers the pulsed lasers to fire when the particle arrives in the mass spectrometer.

We employ a two-laser analysis of the aerosol particles, separating the desorption and ionization steps that typically occur in a single laser pulse in other methods. A pulsed TEA-CO_2 laser (Lumonics) producing 15 to 200 mJ/pulse of radiation near 10.6 μm vaporizes the particle prior to ionization. After a delay of 2−30 μs, a 118.5 nm VUV laser beam, produced by frequency tripling 10 mJ of the 355 nm output of a Nd:YAG laser (Continuum) in a mixture of Xe and Ar gas, ionizes the vapor cloud for time-of-flight mass analysis. The main chamber and the Xe cell are coupled by a LiF lens that recollimates the 355 nm light and loosely focuses the co-propagating 118.5 nm light into the chamber. On the basis of the position of the 355 nm focus in the Xe cell and the curvature of the LiF lens, we calculate a VUV laser spot size of 1 mm^2. The unfocused, residual 355 nm light does not appear to contribute to the signals we observe because no fragment ions resulting from photodissociation of parent ions by the 355 nm light is observed for samples such as aniline, nitrobenzene, or benzyl alcohol. The

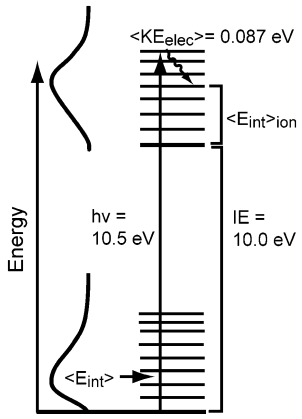

Figure 2. Diagram illustrating the transformation of the neutral thermal energy distribution into an ion internal energy distribution upon photoionization. The ion distribution is broadened to lower energies by the ejection of energetic electrons.

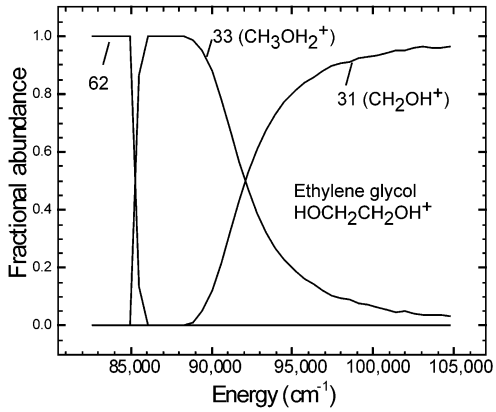

Figure 3. The breakdown diagram of the "thermometer" molecule, ethylene glycol. This is the factional abundance of parent and fragment ions as a function of the ion internal energy. At low energies only the parent ion (*m*/*z* 62) is observed. At an energy of about 85 000 cm^{-1} (10.54 eV) the first fragment (*m*/*z* 33) appears. Above 89 000 cm^{-1} the *m*/*z* 33 and 31 fragment ions are produced competitively.

position of the VUV laser focus is offset from the CO_2 laser focus by a variable distance of 0.25−1 mm along the particle beam axis to account for the motion of the particle center-of-mass, as shown by the inset of Figure 1. We find absolute shot-to-shot intensity fluctuations are only about 15%, likely due to power fluctuations in the VUV laser intensity. A digital oscilloscope digitizes the time-of-flight spectra and transfers them to a PC through a GPIB connection.

The kinetic energy of the vaporized molecules is determined from the mass spectral intensities as a function of the delay between the CO_2 and VUV lasers. In this experiment, the VUV laser spot is displaced approximately 1.5 mm along the time-of-flight axis. The magnitude of the ion signal as a function of delay indicates the time required to traverse this distance. Because the center-of-mass of the aerosol particle has an appreciable velocity (∼100 m/s) normal to the time-of-flight axis, the position of the VUV laser focus along this axis is optimized at each delay, keeping the displacement along the time-of-flight axis constant (1.5 mm). We compare the experimental transients to a model that includes a three-dimensional Maxwell−Boltzmann distribution of velocities, the spot size of our VUV laser (1 mm^2), and the approximate distance along the VUV laser path over which the ionized molecules may be detected (1 cm), to extract approximate translational temperatures for the vaporized molecules.

Analysis

The goal of these studies is the determination of the internal energy of laser-vaporized molecules on the basis of the measured mass spectra. However, the mass spectral intensities reflect the internal energy of the ethylene glycol positive ions produced by the VUV laser, not the neutral gas produced by the CO_2 laser. Hence, recovering the internal energy of the neutral molecules requires (1) relating the mass spectrum to the internal energy for the ions produced by the VUV laser, and (2) mapping the internal energy of the ions onto that for the neutral molecules. Figure 2 shows an energy level diagram of the scheme. Ethylene glycol is a good molecule to use for this study because its ionization potential of 10.0 eV is below, but very close to, the energy of our VUV laser (10.48 eV). Furthermore, the photoionization mass spectrum of ethylene glycol at the energies of this experiment is simple (only 2 fragment ions), and the relative intensities vary significantly as the parent ion internal energy changes.

The 0 K ion "breakdown diagram" generated using photoelectron-photoion coincidence (PEPICO) measurements[18] relates the mass spectrum to the internal energy of the parent ions. The breakdown diagram, shown for ethylene glycol in Figure 3, shows the relative population of the parent ion and each of the fragment ions as a function of the parent ion internal energy. Ethylene glycol ions produced close to the dissociation limit, fragment very slowly, so that the observed onset for fragmentation is a function of how long one waits before mass analysis. That is, the observed onset is instrument dependent. Because the dissociation rate constants were measured in the PEPICO experiment, it was possible to generate the breakdown diagram in Figure 3, which includes the "kinetic shift" appropriate for our aerosol mass spectrometer. The concept and implication of the "kinetic shift" have been thoroughly described in previous work.[19−21] Because the aerosol experiment produces a distribution of ion internal energies, the intensities in a particular experimental mass spectrum do not necessarily correspond to any of the points in the breakdown diagram. Instead, the experimental intensity for the *j*th ion species, I_j, is given by the sum over the breakdown diagram, $B_j(E)$, weighted by the probability distribution of parent ion internal energies, $P(E)$:

$$I_j = \sum_{E'} P(E')B_j(E') \qquad (1)$$

Thus, there is a well-defined relationship between the mass spectrum and the distribution of ion internal energies.

The internal energy of the parent ion, E', has contributions from the internal energy of the neutral precursor, E, the photon energy, $h\upsilon$, the adiabatic ionization energy, IE, and the kinetic energy of the photoelectron, KE_{el} (Figure 2). These are related by conservation of energy by eq 2,

$$E' = E + h\upsilon - IE - KE_{el} \qquad (2)$$

To relate the internal energy of the nascent photoions to their neutral precursors, we assume that Franck-Condon factors for ionization are independent of the neutral internal energy. This approximation has been shown to be valid for several molecules.[22] Because photoionization produces a distribution of photoelectron kinetic energies, the ion internal energy distribution is broader than the corresponding neutral energy distribution. The ion distribution, $P_{ion}(E')$ is determined by convoluting

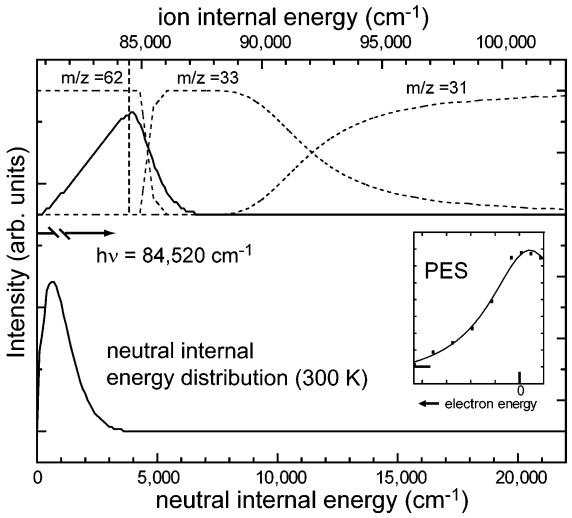

Figure 4. The lower panel shows the internal energy distribution of a room-temperature sample of gaseous ethylene glycol. The inset shows the photoelectron spectrum in the vicinity of the ionization energy. Zero energy indicates the photon energy. The upper panel shows the corresponding ion internal energy distribution along with the ethylene glycol breakdown diagram.

the neutral distribution, $P_{\text{neutral}}(E)$, with the electron kinetic energy distribution, $P_{\text{el}}(\text{KE}_{\text{el}})$, as expressed by eq 3:

$$P_{\text{ion}}(E') = \sum_{E} P_{\text{neutral}}(E) P_{\text{el}}(\text{KE}_{\text{el}}) = \sum_{E} P_{\text{neutral}}(E) P_{\text{el}}(E + h\nu - \text{IE} - E') \quad (3)$$

where KE_{el} is obtained from eq 2. The experimental ethylene glycol electron kinetic energy distribution, or photoelectron spectrum, shown in the inset of Figure 4, has a broad first band with a maximum at 10.55 eV.[23] The portion of the photoelectron spectrum accessed in our experiments (10.0−10.48 eV) is modeled with a Lorentz function fit to the experiment spectrum. Because the vertical ionization energy is very close to the photon energy of 10.48 eV, the Franck−Condon factors for ionization favor the ejection of low-energy electrons so that the ion internal energy distribution is determined mostly by the neutral energy distribution, and not by the distribution of photoelectrons.

The mass spectral intensities for any neutral energy distribution can be predicted using eqs 1−3. In particular, we can test these equations by predicting the spectrum of the room-temperature gas and compare the result to experiment. The bottom panel of Figure 4 shows the room-temperature distribution, calculated using eq 4:

$$P_{\text{neutral}}(E) = \rho(E) \exp(-E/kT) \quad (4)$$

where $\rho(E)$ is the direct-count density of rovibrational states. The upper panel of Figure 4 shows the result of applying eq 3 to this distribution, accounting for the energy of the ionization laser and the distribution of electron kinetic energies. In the figure, this distribution overlays the breakdown diagram for ethylene glycol. Clearly, at room temperature, most of the photoions are created with too little internal energy to fragment, and only a small fraction has sufficient energy to dissociate. Applying eq 1 to this distribution yields the mass spectral intensities, $I_{\text{parent}} = 0.88$, $I_{33} = 0.12$, and $I_{31} = 0.00$, which compare well with the experimental intensities, $I_{\text{parent}} = 0.85$, $I_{33} = 0.15$, and $I_{31} = 0.00$. Increasing the temperature of the neutral distribution by only 30 K from 300 K to 330 K (only a 400 cm^{-1} difference in the average internal energy) results in a mass spectrum that exactly matches the room-temperature experimental spectrum. The slightly larger intensity of the fragment ion in the experiment could arise from (1) a narrower distribution of electron kinetic energies resulting from near-threshold ionization than indicated by the room-temperature He(I) spectrum, (2) a changing photoelectron spectrum as a function of internal energy, or (3) a larger ionization cross section for molecules having higher internal energies. Because there is a geometry change in going from the neutral to the ion,[24] the latter explanation is the most likely one.

One possible approach to describing the internal energy of the vaporized aerosol particles is to find the neutral temperature that best reproduces the experimental mass spectrum. However, we find (especially at high CO_2 laser power), that thermal internal energy distributions do not fit the data because they simultaneously underestimate both the parent and higher-energy fragment ion. As an alternative approach, we build energy distributions using a stochastic fitting method that exactly reproduce our experimental spectra. In this fitting method, the neutral and ion distributions are divided into 100 cm^{-1} wide energy bins, and the neutral distribution is populated with an initial guessed distribution. The final results are found to be insensitive to the shape of the initial distribution (thermal, Gaussian, flat, etc.), but in practice we chose a thermal distribution whose temperature is selected at random and confined to be less than 3000 K. The corresponding ion distribution is calculated using eq 3. The algorithm then chooses a test energy for the neutral molecules at random and adds one unit of population to that energy. To ensure that the neutral and ion distributions are related by eq 3 (as they must be), the stochastic fitting method calculates the corresponding ion energy by first adding the ionization laser energy, $h\nu$, and subtracting from that sum an electron kinetic energy chosen according to probabilities defined by the room-temperature photoelectron spectrum. Adding one unit of population to that ion energy bin and recalculating the mass spectrum according to eq 1 produces a new mass spectrum. If the agreement is better, the program keeps the new point; otherwise, it removes the point from both neutral and ion distributions. When the calculated mass spectrum matches the experimental spectrum, the program repeats the process using a different initial guess distribution and a different random number seed. The program sums the result of 1000 such fitting routines and computes the average internal energy of the neutral distribution. Neither the shape of the model distribution that reproduces the experimental spectrum nor the corresponding average internal energy is unique. However, by generating a large number of model spectra using different random number seeds and different initial guess distributions, we are able to estimate both the average internal energy and its uncertainty. Whereas the error associated with changing Franck-Condon factors (∼30 K) may affect the absolute values of the results, the relative differences between two measurements are more precise. In general, our fitting routine can reliably measure internal energy differences on the order of 10 cm^{-1} (15 K).

Results

Figure 5 shows mass spectra of neat ethylene glycol particles for four different CO_2 laser energies as well as the VUV-ionization mass spectrum of room-temperature ethylene glycol. At the lowest CO_2 laser energy (25 mJ/pulse), the mass spectrum has only two features, the parent ion and its lower-energy fragment, $CH_3OH_2^+$, and the ratio between them is similar to the room-temperature spectrum. This similarity indicates that

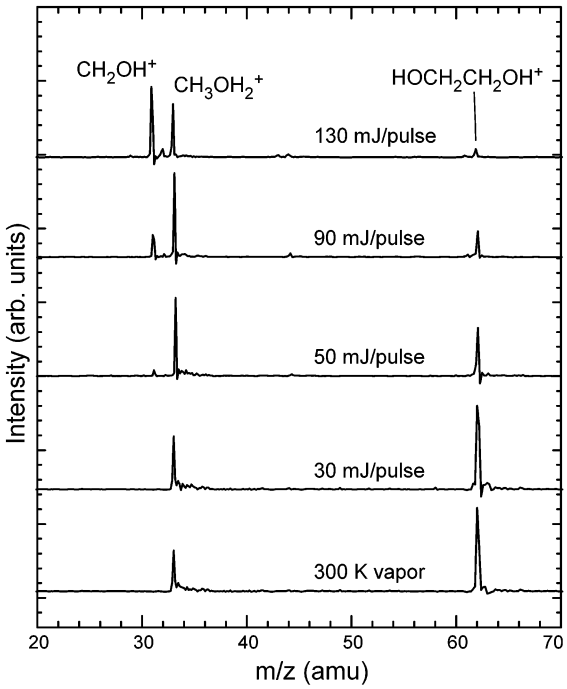

Figure 5. Sample mass spectra of ethylene glycol aerosol particles irradiated with different powers from the CO_2 laser.

the internal temperature of the laser-vaporized molecules is close to room temperature at this CO_2 laser power. Increasing the CO_2 laser power results in a decreased fraction of parent ion and the appearance of the higher-energy fragment ion, CH_2OH^+. At the highest CO_2 laser powers, very little parent ion signal remains and the higher-energy fragment begins to dominate the spectrum. At this high energy, we also observe the CH_3OH^+ ion and the (*m*/*z* 44) ion, but with very little intensity. Although both of these fragment ions were observed in collision-induced dissociation studies,[25] only the (*m*/*z* 44) was observed in the PEPICO study.[24] Because these features only appear at the highest energies and have little intensity, we ignore them in this treatment. The intensities in the mass spectra depend somewhat on the delay between CO_2 and VUV lasers. To minimize errors attributable to either jet or evaporative cooling, the mass spectra were recorded at the shortest delay between the CO_2 and VUV lasers that would produce a good signal (in all cases <2.5 μs).

Applying the stochastic fitting routine to the aerosol mass spectra gives an average internal energy of the laser-vaporized molecules for each CO_2 laser power. Figure 6 shows these data for neat ethylene glycol and a mixture of 1% ethylene glycol in ethanol. Although the energy distributions created with the CO_2 laser are not in thermal equilibrium, it is still useful to relate the internal energies to an equivalent temperature. This is determined by equating the measured average energy, $\langle E \rangle_{\text{exp}}$, to the average energy calculated in eq 5 in which $\rho(E)$ is ethylene glycol density of ro-vibrational states and N is the normalization integral.

$$\langle E \rangle_{\text{exp}} = N^{-1} \int_0^\infty E\rho(E) e^{-E/RT} \, \mathrm{d}E \qquad (5)$$

The left vertical axis in Figure 6 shows the average internal energy calculated from the model, and the right axis shows the corresponding temperature. For neat ethylene glycol, the lowest CO_2 laser power of 25 mJ/pulse produces an average internal energy of 1000 cm^{-1}, similar to the average room-temperature energy. The internal energy increases linearly with CO_2 laser

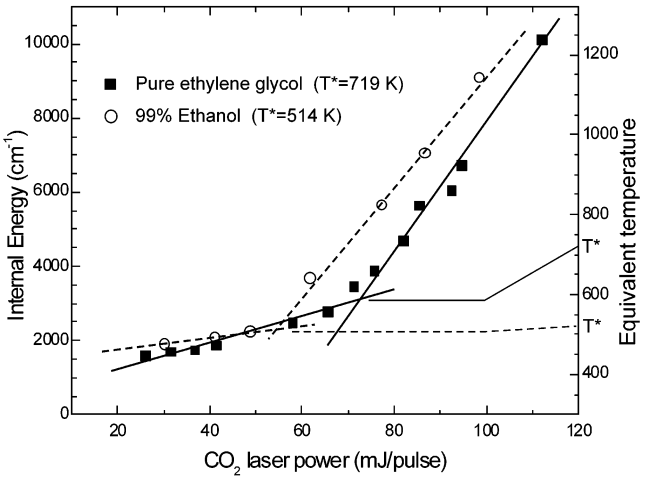

Figure 6. The average internal energy (left ordinate) and equivalent temperature (right ordinate) of pure ethylene glycol particles and particles consisting of 1% ethylene glycol and 99% ethanol derived from the analysis of the ion TOF spectra.

power up to 65 mJ/pulse, at which point the average internal energy is approximately 3100 cm^{-1}. Above that laser power, the internal energy increases much more rapidly with laser power, indicating a drastic change in the vaporization dynamics. As discussed in more detail later in this section, we interpret this change in mechanism as a transition between a slow, layer-by-layer evaporation to a fast explosive or ablative evaporation. At the highest CO_2 laser energy of 110 mJ/pulse, the average internal energy is >10000 cm^{-1} ($T > 1200$ K).

The dilute mixture of ethylene glycol in ethanol produces similar results. A larger background signal in this experiment prohibits recording spectra at very low laser powers; however, the transition from a shallow slope between 30 and 45 mJ/pulse and a steep slope between 45 and 100 mJ/pulse is clearly evident. Whereas the range of internal energies in this system is similar to those in neat ethylene glycol, the transition point occurs at a lower internal energy (2200 cm^{-1} vs 3100 cm^{-1}). Because the two particles have difference macroscopic properties (boiling point, critical temperature, viscosity), a change in the threshold energy (temperature) for ablation is expected. The lower transition temperature for ethanol is most likely a result of its lower boiling point and critical temperature.

As mentioned above, either jet cooling or evaporative cooling can cause the internal energy measured from the mass spectral fragmentation patterns to be lower than the peak internal energy reached just after the application of the laser pulse. To evaluate the extent of this cooling, we determine the internal energy as a function of the delay between the CO_2 and VUV lasers. Figure 7 shows the results of this analysis for two different CO_2 laser powers, 30 mJ/pulse and 90 mJ/pulse. These two laser powers represent the thermal and explosive evaporation dynamics, respectively. In the 90 mJ/pulse experiment, the equivalent internal temperature drops from approximately 615 K to 545 K within 2 μs. Very little cooling occurs beyond 2 μs delay. This steep decline in internal temperature at short delay is likely a result of vibrational cooling in the rapid expansion of the exploding particle. Jet-cooling of the internal degrees of freedom has been observed in other laser vaporization experiments using macroscopic samples.[9,10] The cooling observed for the lower laser power experiment is considerably less, going from 375 to about 340 K. At the lower CO_2 laser power, where the evaporation yields thermal energy distributions, jet cooling is less efficient because the flux from the surface is much lower thereby reducing the number of collisions, which are necessary

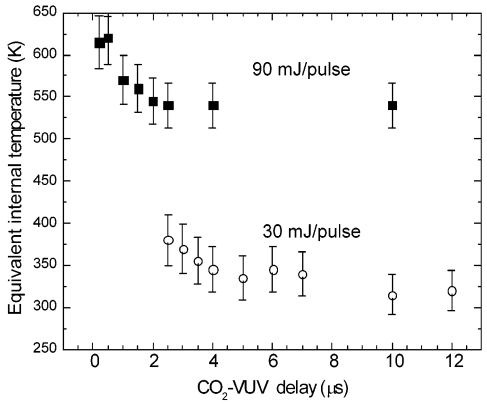

Figure 7. The derived internal temperature at two CO_2 laser pulse energies for various CO_2-VUV laser delays. This shows that the first molecules ejected in the vaporization process have the greatest internal energy.

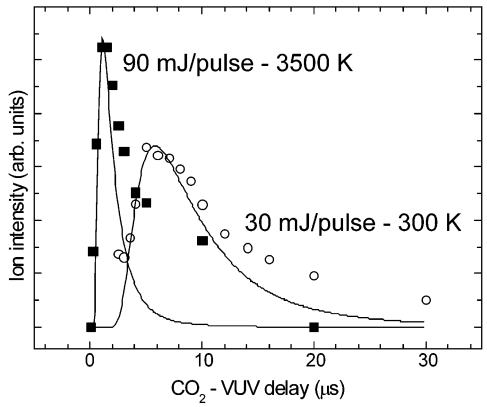

Figure 8. The translational energy distributions of the molecules ejected at low and high CO_2 laser pulse energies.

for jet cooling. In this regime, the cooling is more likely to be evaporative cooling rather than jet cooling. The molecules sampled at the longer delays escaped from the particle after some evaporative cooling had taken place, and their mass spectra reflect the lower temperature of the particle. In the limit of no external heating, molecules evaporating from thin liquid jets of similar dimension to the aerosol particles used in this study have been shown to leave the liquid surface with very few gas-phase collisions.[26]

Figure 8 shows the evolution of the total ion signal (integrated over the whole mass spectrum) as a function of the delay between the CO_2 and VUV lasers for two CO_2 laser powers, 90 mJ/pulse and 30 mJ/pulse. Here, the lasers are arranged with the VUV focus displaced 1.5 mm from the CO_2 laser, as described in the Experimental Section. Since the size of the ionization laser spot is the same in each case, the rate at which the vaporized molecules enter and leave the ionization volume, marked by the rise and loss in signal, is a measure of their kinetic energy. Clearly, at the lower energy, the molecules take longer to reach the ionization volume ($\sim$10 μs) than in the high power case ($\sim$2 μs). Comparing these experimental transients to a model that includes a three-dimensional Maxwell−Boltzmann distribution of velocities yields approximate translational temperatures for the vaporized molecules. We estimate these temperatures to be 300 and 3500 K, respectively. The former number is very similar to the internal temperature measured at that laser power, whereas the latter is much higher than the corresponding internal temperature. The large difference between the internal and translational temperatures indicates that internal energy is converted into translational energy as in a supersonic expansion. As pointed out above, more vibrational cooling at high laser power is expected because the vapor flux from the particle surface is much higher, resulting in more collisions. Both the low and high CO_2 laser power transients have more intensity at longer delay than the Maxwell−Boltzmann model predicts. In the case of explosive evaporation, this slow component of the signal may be attributed to the continuing evaporation in the tail of the CO_2 laser pulse of cold nanodroplets created in the initial burst. The slow signal in the thermal regime can be explained by the continuing evaporation of the droplet whose temperature has been reduced by evaporative cooling. In both cases, we ignored this slow component of signal for the Boltzmann model.

Discussion

These results demonstrate that the mass spectral fragmentation pattern of ethylene glycol may be used as a probe of internal energy corresponding to temperatures just above room temperature to over 1200 K. The impact of these results is 2-fold. First, these results provide new information regarding the mechanism of laser vaporization of aerosol particles. Specifically, we observe that the efficiency with which the laser deposits internal energy in the vaporized molecules increases dramatically beyond the threshold value where the vaporization mechanism changes from thermal to explosive.

Most laser desorption processes occur in the limit of thermal confinement.[27,28] This condition arises when the laser pulse duration, τ_p, is shorter than the time for thermal equilibration, $\tau_{th} \sim L_p^2 / D_T$, where L_p is the size of the absorbing structure (the aerosol particle) and D_T is the thermal diffusivity of the material. Since τ_{th} is on the order of 10 μs and τ_p 1 μs for the 2-μm particles used in this study, the limit of thermal confinement applies in our case, as well. As a result, the CO_2 laser may heat the particle well beyond its normal boiling temperature. The evaporation dynamics change from a purely surface evaporation at low laser fluences to an explosive evaporation, or phase explosion, of the superheated particle at high fluences. Several imaging experiments directly illustrate this transition from thermal to explosive vaporization.[1] Likewise, a number of other experiments show indirect evidence of this change in evaporation mechanism, including depth-profiling measurements[6] and "ion evaporation" measurements.[29] Although the threshold power for explosive vaporization depends on a number of factors (including the identity of the material, the characteristics of the laser, the size of the particle, etc.), several studies show that this threshold is on the order of 1×10^6 W/cm^2 for CO_2 laser ablation.[1,3,30,31] Because the laser power at which we observe the change in heating rate is well-correlated with other observations of the onset of explosive vaporization, it appears that the increased heating rate is another manifestation of this change in mechanism.

The reason for the increased efficiency of internal energy deposition after the onset of explosive vaporization is not immediately clear. One explanation is that explosive vaporization is correlated with reaching supercritical temperatures within the ethylene glycol droplet. At critical temperature, the heat of evaporation is zero so that less internal energy needs to be converted into translational energy for the molecules to evaporate. Thus, more energy appears as internal energy. This hypothesis is born out by the experiment using dilute ethylene glycol in ethanol. Because the transition to a higher heating rate occurs at a lower temperature than for neat ethylene glycol, this transition is a property of the matrix rather than of ethylene glycol. Both the critical temperature and normal boiling point

of ethanol are lower than for ethylene glycol, suggesting that the transition is associated with these properties. The internal temperature at the transition in ethylene glycol to explosive vaporization (610 K) is lower than the critical temperature of 710 K.[32] This discrepancy may be explained by vibrational cooling in the rapid expansion, as has been observed in previous ablation studies,[9,10] and measured directly in this work. The evaporating molecules undergo collisions with the surrounding vapor molecules that convert internal energy into translational energy prior to ionization by the VUV laser. This assertion is consistent with the observation that the approximate translational temperature is much greater than the internal temperature for CO_2 laser powers above the explosive vaporization threshold. In the case of the ethanol data, the break in the slope at 500 K is very close to the ethanol critical temperature of 514 K.[32]

The second aspect of these results in this range of internal temperatures is their usefulness in probing the initiation steps of explosive combustion reactions in aerosols.[7] Ethylene glycol can easily be added to any neat liquid system in which it is soluble, prior to creating the aerosol particles. Adding it to solid systems requires co-dissolving the explosive fuel and ethylene glycol in a volatile solvent, creating an aerosol from the solution, and allowing the solvent to evaporate. During the explosive reaction initiated by the pulsed IR laser, the ethylene glycol is in thermal equilibrium with the reacting system, and its photoionization mass spectrum provides a measure of the reaction temperature. There are other considerations that may limit its utility as a "thermometer" and chief among them is its reactivity. Ethylene glycol may be added to the reactive systems in very low concentrations ($\sim$0.01 vol %) and still be easily detected, thereby reducing the likelihood of a significant chemical interaction. On the other hand, trace concentrations of impurities are known to have drastic effects on some explosive combustion reactions. For example, small concentrations ($\sim$0.1%) of amines "sensitize" the explosive reaction of nitroalkyl compounds.[7,33−36] It is straightforward to perform the explosive combustion experiments with and without the trace ethylene glycol to ensure that the results are consistent. A more important limitation is the cooling of the vibration modes, especially in the explosive vaporization limit. When this vibrational cooling exists, the internal energy measured from the mass spectra reflect a lower limit to the "real" or peak internal energy reached by the superheated particle. The limitation may be partially overcome by using the smallest possible delay between the CO_2 and VUV lasers.

Conclusions

The internal energy of ethylene glycol vapor created in the CO_2 laser vaporization of neat ethylene glycol aerosol particles in a vacuum has been measured by analyzing VUV photoionization mass spectra of the vapor plume using "breakdown diagrams" extracted from PEPICO data. The internal energy varies from 1300 to 10250 cm^{-1} over a range of CO_2 laser fluences from 25 to 110 mJ/pulse. The data also show a sharp rise in the rate of increase of the internal energy with respect to CO_2 laser power near 65 mJ/pulse. The change is correlated with a change in vaporization mechanism from thermal to explosive vaporization. The increase in the heating rate may be attributable to the vanishing heat of vaporization of particles heated to and beyond their critical temperatures. The translational energy of the vaporized molecules was determined by examining the total ion signal as a function of the delay between the CO_2 and VUV lasers. The translational energy at high laser power is much higher than the internal energy, implying that there is some cooling of the vibrational modes in the rapid gas expansion. Because of the simplicity of the mass spectra, ethylene glycol may be used as a "chemical thermometer" for reactions in aerosol particles in this internal energy range, though vibrational cooling may limit the accuracy of such a method. This approach can also be used to measure the internal energy in other ionization processes, such as MALDI, simply by adding a small amount of ethylene glycol to the matrix.

Acknowledgment. We thank the Air Force Office of Scientific Research for the support of this work.

References and Notes

(1) Latifi, H.; Xie, J.-G.; Ruekgauer, T. E.; Armstrong, R. L.; Pinnick, R. G. *Opt. Lett.* **1991**, *16*, 1129.
(2) Park, B.-S.; Biswas, A.; Armstrong, R. L. *Opt. Lett.* **1990**, *15*, 206.
(3) Pinnick, R. G.; Biswas, A.; Armstrong, R. L.; Jennings, S. G.; Pendleton, J. D.; Fernandez, G. *Appl. Opt.* **1990**, *29*, 918.
(4) Schoolcraft, T. A.; Constable, G. S.; Zhigilei, L. V.; Garrison, B. J. *Anal. Chem.* **2000**, *72*, 5143.
(5) Schoolcraft, T. A.; Constable, G. S.; Jackson, B.; Zhigilei, L. V.; Garrison, B. J. *Nucl. Instrum. Methods Phys. Res., Sect. B* **2001**, *180*, 245.
(6) Woods, E., III; Smith, G. D.; Miller, R. E.; Baer, T. *Anal. Chem.* **2002**, *74*, 1642.
(7) Woods, E., III; Dessiaterik, Y.; Miller, R. E.; Baer, T. *J. Phys. Chem. A* **2001**, *105*, 8273.
(8) Mowry, C. D.; Johnston, M. V. *J. Phys. Chem.* **1994**, *98*, 1904.
(9) Zhang, J.-Y.; Nagra, D. S.; Li, L. *Anal. Chem.* **1993**, *65*, 2812.
(10) Elokhin, V. A.; Krutchinsky, A. N.; Ryabov, S. E. *Chem. Phys. Lett.* **1990**, *170*, 193.
(11) Cousins, L. M.; Levis, R. J.; Leone, S. R. *J. Phys. Chem.* **1989**, *93*, 5325.
(12) Woods, E., III; Smith, G. D.; Dessiaterik, Y.; Baer, T.; Miller, R. E. *Anal. Chem.* **2001**, *73*, 2317.
(13) Carson, P. G.; Neubauer, K. R.; Johnston, M. V.; Wexler, A. S. *J. Aerosol Sci.* **1995**, *26*, 535.
(14) Murphy, D. M.; Thomson, D. S. *Aerosol Sci. Technol.* **1995**, *22*, 237.
(15) Prather, K. A.; Nordmeyer, T.; Salt, K. *Anal. Chem.* **1994**, *66*, 1403.
(16) Liu, P.; Ziemann, P. J.; Kittelson, D. B.; McMurry, P. H. *Aerosol Sci. Technol.* **1995**, *22*, 293.
(17) Liu, P.; Ziemann, P. J.; Kittelson, D. B.; McMurry, P. H. *Aerosol Sci. Technol.* **1995**, *22*, 314.
(18) Sztaray, B.; Baer, T. *J. Am. Chem. Soc.* **2000**, *122*, 9219.
(19) Chupka, W. A. *J. Chem. Phys.* **1959**, *30*, 191.
(20) Huang, F. S.; Dunbar, R. C. *J. Am. Chem. Soc.* **1990**, *112*, 8167.
(21) Lifshitz, C. *Mass Spectrom. Rev.* **1982**, *1*, 309.
(22) Hoogerbrugge, R.; Bobeldijk, M.; Los, J. *J. Phys. Chem.* **1989**, *93*, 5444.
(23) Kimura, K.; Katsumata, S.; Achiba, Y.; Yamazaki, T.; Iwata, S. *Handbook of He(I) Photoelectron Spectra of Fundamental Organic Molecules*; Halsted Press: New York, 1981.
(24) Li, Y.; Baer, T. *J. Phys. Chem. A* **2002**, *106*, 8656.
(25) Burgers, P. C.; Holmes, J. L.; Hop, C. E. C. A.; Postma, R.; Ruttink, P. J. A.; Terlouw, J. K. *J. Am. Chem. Soc.* **1987**, *109*, 7315.
(26) Faubel, M.; Schlemmer, S.; Toennies, J. P. *Z. Phys. D: At., Mol. Clusters* **1988**, *10*, 269.
(27) Miotello, A.; Kelly, R. *Appl. Phys. A* **1999**, *A69*, S67−S73.
(28) Zhigilei, L. V.; Garrison, B. J. *J. Appl. Phys.* **2000**, *88*, 1281.
(29) Dessiaterik, Y.; Woods, E., III; Nguyen, T. G.; Smith, G. D.; Miller, R. E.; Baer, T. Manuscript in preparation.
(30) Alexander, D. R.; Armstrong, J. G. *Appl. Opt.* **1987**, *26*, 533.
(31) Singh, P. I.; Knight, C. J. *AIAA J.* **1980**, 18, 96.
(32) Lide, D. R. *CRC Handbook of Chemistry and Physics*; CRC Press: Boca Raton, FL, 2000.
(33) Constantinou, C. P.; Mukundan, T.; Chaudhri, M. M. *Philos. Trans. R. Soc. London, Ser. A* **1992**, *339*, 403.
(34) Gruzdkov, Y. A.; Gupta, Y. M. *J. Phys. Chem. A* **1998**, *102*, 2322.
(35) Pangilinan, G. I.; Gupta, Y. M. Molecular processes in a shocked explosive: time-resolved spectroscopy of liquid nitromethane. High-Pressure Shock Compression Solids III. Conference Proceeding, 1998.
(36) Politzer, P.; Seminario, J. M.; Zacarias, A. G. *Mol. Phys.* **1996**, *89*, 1511.